Vehicle System Dynamics: International Journal of Vehicle Mechanics and Mobility
Publication details, including instructions for authors and subscription information:
http://www.tandfonline.com/loi/nvsd20

A path-following driver-vehicle model with neuromuscular dynamics, including measured and simulated responses to a step in steering angle overlay

David J. Cole [a]
[a] Department of Engineering , University of Cambridge , Trumpington Street, Cambridge , CB2 1PZ , UK
Published online: 09 Sep 2011.

To cite this article: David J. Cole (2012) A path-following driver-vehicle model with neuromuscular dynamics, including measured and simulated responses to a step in steering angle overlay, Vehicle System Dynamics: International Journal of Vehicle Mechanics and Mobility, 50:4, 573-596, DOI: 10.1080/00423114.2011.606370

To link to this article: http://dx.doi.org/10.1080/00423114.2011.606370

Vehicle System Dynamics
Vol. 50, No. 4, April 2012, 573–596

Taylor & Francis
Taylor & Francis Group

A path-following driver–vehicle model with neuromuscular dynamics, including measured and simulated responses to a step in steering angle overlay

David J. Cole*

Department of Engineering, University of Cambridge, Trumpington Street, Cambridge CB2 1PZ, UK

(*Received 28 December 2010; final version received 14 July 2011*)

An existing driver–vehicle model with neuromuscular dynamics is improved in the areas of cognitive delay, intrinsic muscle dynamics and alpha–gamma co-activation. The model is used to investigate the influence of steering torque feedback and neuromuscular dynamics on the vehicle response to lateral force disturbances. When steering torque feedback is present, it is found that the longitudinal position of the lateral disturbance has a significant influence on whether the driver's reflex response reinforces or attenuates the effect of the disturbance. The response to angle and torque overlay inputs to the steering system is also investigated. The presence of the steering torque feedback reduced the disturbing effect of torque overlay and angle overlay inputs. Reflex action reduced the disturbing effect of a torque overlay input, but increased the disturbing effect of an angle overlay input. Experiments on a driving simulator showed that measured handwheel angle response to an angle overlay input was consistent with the response predicted by the model with reflex action. However, there was significant intra- and inter-subject variability. The results highlight the significance of a driver's neuromuscular dynamics in determining the vehicle response to disturbances.

Keywords: neuromuscular; steering; driver; reflex; muscle; torque; control; active; overlay

1. Introduction

There is currently strong interest in the use of advanced steering technology to improve the safety, performance and efficiency of road vehicles. Sophisticated systems that actively modify the steering angle and torque are now in production. Much of the development work is performed using test drivers and prototype vehicles. A consequence is that product development is time-consuming and expensive and the technology may not be exploited to its full potential. Elsewhere in the vehicle engineering process, mathematical models are used extensively to support decision-making during the low-cost design phase. An absence of significant theoretical understanding of human steering control

*Email: djc13@cam.ac.uk

ISSN 0042-3114 print/ISSN 1744-5159 online

http://dx.doi.org/10.1080/00423114.2011.606370
http://www.tandfonline.com

behaviour is thought to be limiting the use of mathematical simulation in the design of steering system dynamics. The Driver–Vehicle Dynamics Group at Cambridge University Engineering Department [1] has been working to develop improved driver models, with the aim of moving some of the vehicle development activity to the low-cost design phase.

The main area of study in this paper is the effect of steering torque feedback on the dynamic response of the driver–vehicle system. The effect of steering torque feedback can be considered in two parts: (i) the mechanical response of the arm inertia, muscles and reflexes and (ii) the cognitive response of the brain to the sensed torque at the handwheel. Kim and Cole [2,3] have undertaken a preliminary investigation into the driver's cognitive use of the sensed steering torque. The present paper focusses on the effect of steering torque feedback on the mechanical response.

One of the earliest attempts to understand the role of neuromuscular dynamics in the driver–vehicle–steering system was by Modjtahedzadeh and Hess [4]. Building upon their work, Pick and Cole [5–10] developed a driver–vehicle model for simulating a path-following task at constant vehicle speed. The model included the driver's neuromuscular system comprising arm inertia, muscles and stretch reflex dynamics. The ability of the driver to stiffen the arms by co-contracting muscles was investigated experimentally [7–9]. The model was used to demonstrate that stiffening the muscles, despite consuming energy, was an optimal strategy when the driver's knowledge of the steering torque feedback behaviour was inaccurate [10].

Hoult [11] and Hoult and Cole [12] continued the work of Pick and Cole, focussing particularly on measuring and modelling the intrinsic muscle dynamics. Odhams [13] and Odhams and Cole [14] performed experiments on a driving simulator to identify models of path-following control; they concluded that a preview control model [15] was appropriate. More recently, Droogendijk [16] and Katzourakis *et al.* [17] developed driver–vehicle models incorporating neuromuscular dynamics, paying special attention to alpha–gamma co-activation of the muscle and reflexes. Sentouh *et al.* [18] presented a driver–vehicle model incorporating steering torque feedback, but reflex dynamics were not included explicitly.

The present paper extends the driver model of Pick and Cole [10] with an improved model of intrinsic muscle dynamics developed recently by Hoult [11] and Hoult and Cole [12]. They found that the intrinsic muscle dynamics are dominated by a damping term at low frequency, whereas previous studies [10,16,17] have employed models in which low frequency behaviour is dominated by a stiffness term; this is thought to have arisen because of the difficulty associated with identifying experimentally the separate contributions of the intrinsic, reflex and cognitive dynamics. Improvements are also made to modelling of the cognitive delay and the alpha–gamma co-activation; in particular, the inverse model used in [10,16,17] to generate the co-activation signal is replaced by a forward model. Of special interest in the present paper is understanding of the way in which the neuromuscular system in combination with steering torque feedback affects the response of the vehicle to external lateral disturbances and to steering angle and torque overlay inputs. The next section of the paper describes the neuromuscular and vehicle model and highlights the improvements made in comparison to the earlier models. The behaviour of the model in a path-following task is described in Section 3. Torque overlay and angle overlay steering functions are added to the vehicle model in Section 4. Experiments using a fixed-base driving simulator are described in Section 5 and compared with predictions of the model. Conclusions and suggestions for further work are given in the final section of the paper. Early results of this work were presented in Cole and Hoult [19,20].

2. Neuromuscular and vehicle model

2.1. *Structure*

The structure of the driver–vehicle model is shown in Figure 1. The model represents a path-following task in the linear operating regime of the vehicle and at constant vehicle speed. Block H_v is the vehicle, H_s is the steering, H_a and H_b are the muscle dynamics, and H_r and D_r are the stretch reflex dynamics. These blocks comprise the system to be controlled by the driver's brain, which is represented by blocks K, D_c and H_f. The brain generates the alpha–gamma control signals denoted by α and γ. The following subsections describe the blocks and their interconnections in more detail.

2.2. *Vehicle*

The vehicle (H_v) is represented using the well-known linear lateral–yaw two-wheel vehicle model shown in Figure 2. All the parameters and their default values are given in Table 1. The default parameter values represent a passenger car with 50/50 mass distribution, unity dynamic index ($I = \text{mab}$) and neutral steer characteristic. The constant vehicle speed is U. The control input to the vehicle is the pinion angle θ. The front road wheel steer angle δ is equal to the pinion angle θ divided by the steering gear ratio G. In addition to the tyre forces, external disturbance forces acting on the vehicle mass are lateral forces acting at the centre of mass (F_d), front axle position (F_f) and rear axle position (F_r) as shown in Figure 2. States are the lateral and yaw velocities v and ω in vehicle-fixed axes. The equations of motion are

$$m(\dot{v} + U\omega) = C_r\frac{b\omega - v}{U} + C_f\frac{-a\omega - v}{U} + C_f\delta + F_r + F_d + F_f, \tag{1}$$

$$I\dot{\omega} = -bC_r\frac{b\omega - v}{U} + aC_f\frac{-a\omega - v}{U} + aC_f\delta + bF_r + aF_f. \tag{2}$$

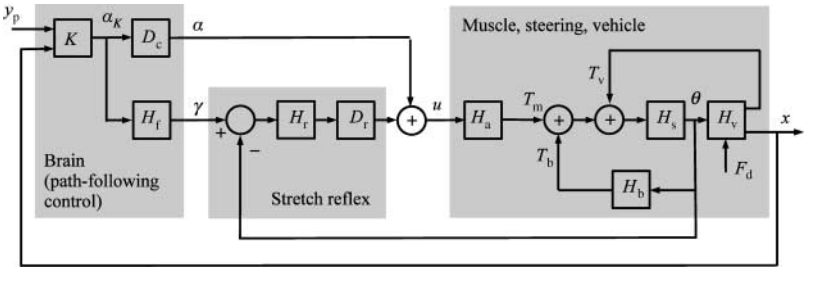

Figure 1. Structure of the driver–vehicle model.

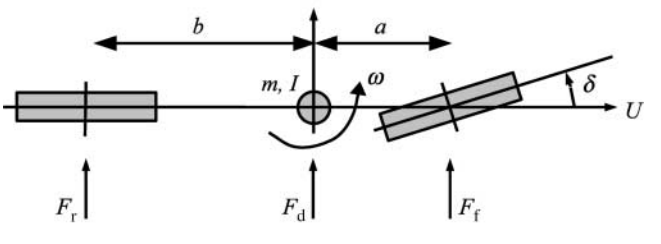

Figure 2. Vehicle model with external disturbance forces acting at the centre of mass (F_d), front axle position (F_f) and rear axle position (F_r).

Table 1. Parameter values of driver–vehicle model.

Speed	U	30 m/s
Steering gear ratio	G	16
Trail	d	0 or 75 mm
Mass	m	1500 kg
Front axle distance	a	1.25 m
Rear axle distance	b	1.25 m
Front axle cornering stiffness	C_f	150 kN/rad
Rear axle cornering stiffness	C_r	150 kN/rad
Steering inertia	I_pinion	0.02 kg m^2
Arms and handwheel inertia (relax or tense)	$I_\mathrm{arm} + I_\mathrm{hw}$	0.055 or 0.071 kg m^2
Steering stiffness	k_s	2.0 N m/rad
Steering damping	c_s	2.0 N m s/rad
Intrinsic muscle stiffness (relax or tense)	k_p	0 or 0 N m/rad
Intrinsic muscle damping (relax or tense)	c_p	1.17 or 1.97 N m s/rad
Intrinsic muscle stiffness (relax or tense)	k_a	0 or 5.0 N m/rad
Intrinsic muscle damping (relax or tense)	c_a	0 or 1.25 N m s/rad
Reflex gain	k_r	0 or 50 N m/rad
Reflex delay	t_r	0.04 s
Cognitive delay	t_c	0.5 s
Preview time	t_p	3 s
Discrete-time step	t_s	0.005 s
Cost function weight	q_1	10^5
Cost function weight	q_2	10^5

For the purpose of calculating the lateral displacement of the vehicle relative to a ground-fixed axis, it is assumed that the yaw angle ψ of the vehicle relative to a ground-fixed axis remains small. The lateral displacement y is then determined by integrating the lateral velocity $\dot{y} = v + U\psi$ relative to the ground-fixed axis. Pinion torque T_v arises from the lateral front tyre force acting at distance d behind the point where the kingpin axis intercepts the ground (mechanical plus pneumatic trail).

The model assumes that lateral tyre force is proportional to tyre slip angle. For real tyres, lateral force is not generated instantaneously in response to changes in slip angle; relaxation behaviour of the tyre means that there is an approximately first-order lag between slip angle and lateral force, the time constant of which depends on the tyre design, vehicle speed and other operating conditions [21]. Relaxation length for a typical car tyre is 0.5 m, which at a vehicle speed of 30 m/s corresponds to a time constant of 17 ms, but can be significantly shorter [21]. This time constant is shorter than other time constants to be included in the driver–vehicle model and therefore the tyre relaxation behaviour is not included in the model.

Figure 3 shows the yaw velocity response ω and the torque T_v acting on the pinion (from the rack) to a unit step (one radian) in pinion angle θ for a vehicle speed $U = 30$ m/s. The yaw velocity settles to 0.75 rad/s. The pinion torque response jumps immediately to -44 Nm, which arises from the lateral front axle force of 9375 N generated when one radian divided by the gear ratio $G = 16$ appears as a slip angle on the front axle with cornering stiffness $C_\mathrm{f} = 150$ kN/rad. The pinion torque then moves towards zero for a short time before approaching its steady-state value of -79 Nm. This value of pinion torque arises from the force generated at the front axle during steady turning. The 'stiffness' seen at the pinion due to the lateral tyre force arising from steady cornering is thus 79 Nm/rad for a vehicle speed of $U = 30$ m/s. Note that a unit step in pinion angle would not normally be applied in practice at this vehicle speed, since the corresponding steady-state lateral vehicle acceleration is 22.5 m/s^2.

Figure 4 shows lateral displacement y and pinion torque T_v responses to lateral impulsive force disturbances of magnitude 500 Ns at the centre of mass (solid line), front axle position (dash) and rear axle position (dash-dot). In these responses, the pinion angle θ and road wheel

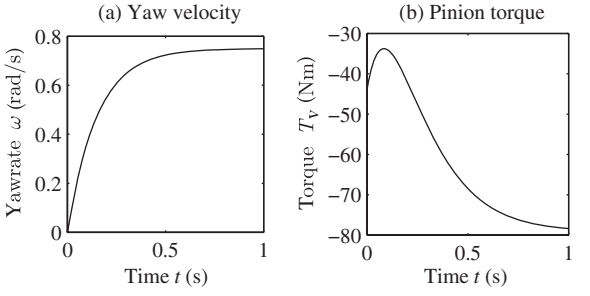

Figure 3. Yaw velocity and pinion torque response of the vehicle to a one radian step in pinion angle, vehicle speed $U = 30$ m/s.

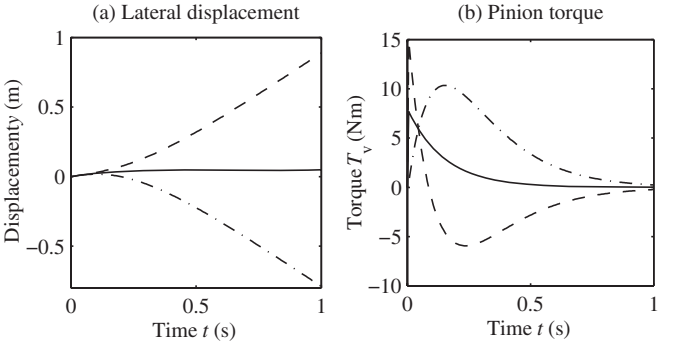

Figure 4. Lateral displacement and pinion torque responses of the vehicle to 500 Ns impulsive disturbances in F_d (solid), F_f (dash) and F_r (dash-dot).

steer angle δ remain zero. When the impulse occurs at the centre of mass (F_d, solid line), the vehicle moves laterally by 50 mm but then continues travelling in the original direction; the position of the disturbance and the neutral steer characteristic of the vehicle mean that the yaw velocity response ω remains zero. The maximum pinion torque is about 7.7 Nm. When the impulse occurs at the front axle position (F_f, dashed), the vehicle eventually travels away from the original direction of travel at a rate of $\dot{y} = 1.2$ m/s due to the impulsive yaw moment about the centre of mass in the positive yaw direction. The pinion torque instantaneously reaches 15 Nm, but then changes sign to reach -6 Nm before settling to zero. When the impulse occurs at the rear axle position (F_r, dash-dot), the vehicle is initially displaced in the positive y direction but because the impulsive yaw moment now acts in the negative yaw direction, the vehicle eventually travels away from the original direction of travel at a rate of -1.2 m/s. The pinion torque starts at zero, reaches 10 Nm, then settles back to zero. It will be seen in later sections of the paper that this strong dependence of the pinion torque response on the position of the lateral disturbance has a significant influence on the driver's ability to compensate for the disturbance.

2.3. *Muscle and steering*

The muscle and steering model comprises the three blocks labelled H_s, H_a and H_b, see Figure 1. Figure 5(a) shows the structure of H_s which represents an unassisted mechanical steering system and the inertia of the driver's arms. The inertia of the steering system (comprising the handwheel I_{hw}, column, rack and pinion gear, front wheels and other steered components), referenced to the pinion axis, is denoted by I_s. This inertia is connected to the vehicle ground

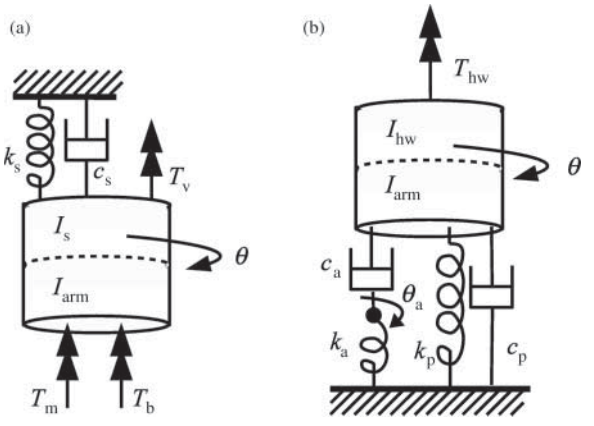

Muscle and steering model with one rotational degree of freedom for transfer function H_s in Figure 1.

Mechanistic model of intrinsic muscle behaviour, with two rotational degrees of freedom, used to generate model frequency responses shown in Figure 6.

Figure 5. Muscle models.

by a torsional stiffness k_s that represents self-centring stiffness (typically arising from the weight of the vehicle acting through the suspension and steering geometry) and a parallel torsional damper c_s to represent damping in the mechanism. The pinion torque T_v (defined in the preceding subsection) arising from the lateral tyre force acts on the steering inertia. The inertia of the driver's arms referenced to the pinion axis is denoted I_{arm} and is assumed to be rigidly connected to the handwheel (denoted by the dotted line between I_{arm} and I_s in Figure 5(a)). The arm muscles apply torque to the arm inertia. The muscle torque consists of two components, T_m and T_b, described in the next paragraphs. The equation of motion is

$$(I_s + I_{arm})\ddot{\theta} + c_s\dot{\theta} + k_s\theta = T_m + T_b + T_v. \tag{3}$$

This system is embodied in the transfer function H_s, whose input is the total torque (T_m, T_b and T_v) acting on the inertia and the output is the pinion angle θ. The handwheel angle is assumed equal to the pinion angle, except when the angle overlay is introduced in Section 4.

The muscle torque component T_b arises from the internal stiffness and damping of the muscles and joints, known as the intrinsic torque. The intrinsic torque T_b is related to the handwheel angle θ by the transfer function H_b. The transfer function is strongly dependent on the activation level of the muscle. Hoult [11] has identified this transfer function for a range of drivers with muscles tensed (co-contracted) and with muscles relaxed. The transfer functions were identified using a torque-controlled servo motor directly connected to a handwheel. The test subject held onto the handwheel, while a random torque was generated by the servo motor. The torque, angular displacement and velocity were all measured at the hub of the handwheel and used to identify a parametric model (Box–Jenkins). Great care has to be taken to avoid errors in the identification arising from unavoidable neural activation of the muscle and from neural noise, see [11] for details.

The solid and dash-dot lines in Figure 6 show the transfer functions identified by Hoult [11] for one test subject in tensed (solid) and relaxed (dash-dot) conditions. T_{hw} is the torque measured at the hub of the handwheel and $\dot{\theta}$ is the angular velocity of the handwheel. Note that these identified transfer functions are not entirely consistent with the definition of H_b in Figure 1. First, the transfer functions are shown for angular velocity ($\dot{\theta}$) input, not displacement

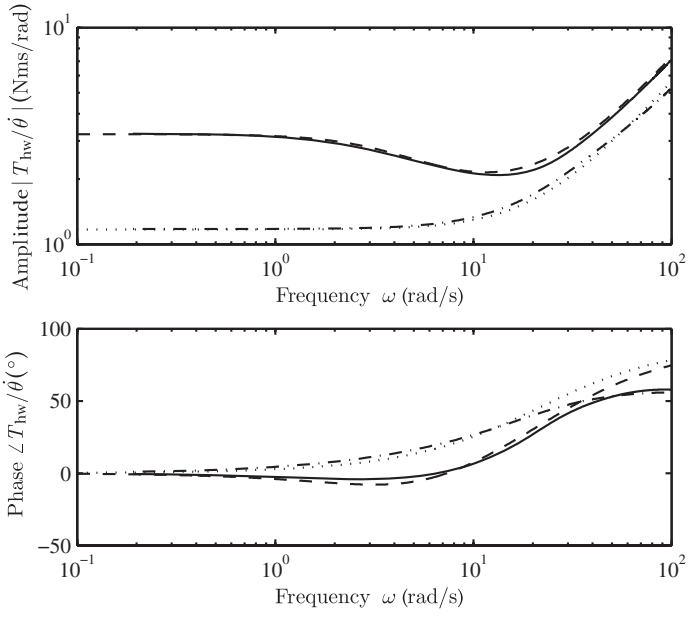

Figure 6. Frequency responses of driver's arms identified by Hoult [11] for tensed (solid) and relaxed (dash-dot) conditions. Frequency responses of a mechanistic model are shown for tensed (dashed) and relaxed (dotted) conditions.

(θ). Second, the transfer functions include the effect of inertia of the handwheel and arms, inertia which in Figure 1 is included in block H_s and not H_b.

The inertia of the arms and handwheel $I_{arm} + I_{hw}$ gives rise to the 20 dB/decade slope of the identified transfer functions at high frequency. At low frequency, the transfer functions have zero slope, which suggests a predominantly damping characteristic at low frequency.

The identified gain at low frequency increases when the muscles are tensed (co-contracted). This can be ascribed to the greater number of cross-links that are made in the muscle fibres when the muscle is activated strongly. There is also a slight increase in gain at high frequencies, and since the response in this frequency region is dominated by the inertia of the arms and handwheel, it is likely that tensed arm muscles lead to increased participation of the inertia of the upper arms and torso [11].

The simple mechanistic model shown in Figure 5(b) was fitted to Hoult's parametric model. The equations of motion are

$$(I_{arm} + I_{hw})\ddot{\theta} + (c_a + c_p)\dot{\theta} + k_p\theta = T_{hw} + c_a\dot{\theta}_a, \tag{4}$$

$$c_a\dot{\theta}_a + k_a\theta_a = c_a\theta. \tag{5}$$

Frequency responses of the model are shown in Figure 6 for tensed (dashed) and relaxed (dotted) conditions. The torsional spring and damper elements of the mechanistic model specify transfer function H_b in Figure 1. Parameter values are given in Table 1.

The muscle torque component T_m arises from the neural activation of the muscle. There are three processes associated with the activation block H_a in Figure 1. Activation begins with a signal u sent to alpha motor neurons in the spine that in turn activate the muscle fibres. The dynamics associated with the motor neurons are represented by a first-order lag with time constant in the range 20–50 ms [11]. In the present work, a value of 30 ms is used. There is also a lag associated with the activation and deactivation of the muscle fibres. Twitch tests on muscles suggest the activation time constant is in the range 5–15 ms, whereas deactivation is

slower, typically 20–60 ms, depending on the size of the muscle [22]. In the present work, a first-order lag with time constant of 20 ms is used for both activation and deactivation. Finally, the muscle fibres have some series compliance, principally due to the tendons. The effect of this compliance is modelled as another first-order lag with time constant 50 ms. The three time constants are considered to be independent of the activation level of the muscles [11]. The series combination of the three first-order lags define the H_a block in Figure 1. The block has unity gain and zero phase at zero frequency.

Figure 7(a) shows transfer functions of the muscle and steering system only, comprising blocks H_s, H_a and H_b. For the dash-dot line and the dotted line, the input is muscle activation signal u (nominal units Nm) and the output is pinion (handwheel) angle θ in radians. The dash-dot line corresponds to the muscles in the tensed (co-contracted) condition and the dotted line is the relaxed condition. The vehicle H_v is not present and so the input from the pinion torque T_v is zero; the driver is in effect sitting in a stationary car with the front wheels on a zero friction surface. The driver holds onto the steering wheel and activates the muscle. At very low frequencies, the system behaves like an inertia ($I_{arm} + I_s$) on a soft spring ($k_s + k_p$), the gain (0.5 rad/Nm) is therefore the reciprocal of the spring stiffness (2 Nm/rad). At very high frequency, the gain roll-off is -100 dB/decade, which arises from the inertia (-40 dB/decade) and the three first-order lags (-20 dB/decade each) in the path from u to θ. The changes in slope in the intermediate frequency range are consistent with the time lags and corner frequencies of the system, the effect of the inertia occurring first (in the region of 1–10 rad/s) followed by the activation lags (20–50 rad/s). The relaxed muscles (dotted) give larger gain over much of the frequency range because they offer less damping and inertia. At very low frequencies, the gains for the relaxed and tensed conditions are the same because in both conditions the muscle model has no stiffness at low frequency, see Figure 6.

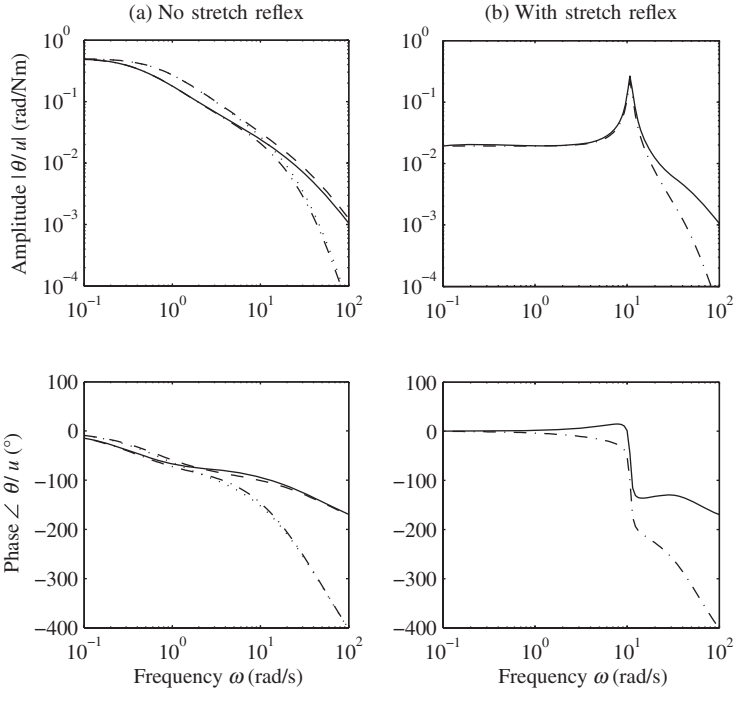

Figure 7. Frequency responses of muscle and steering model. Pinion torque input T_m or T_v: tensed (solid), relaxed (dashed). Activation signal input u: tensed (dash-dot) and relaxed (dotted).

Figure 7(a) also shows two transfer functions of the muscle and steering system, excluding the activation block H_a. The input is torque applied to the pinion (either T_m or T_v) and the output is pinion angle θ. The solid line corresponds to the tensed muscle and the dashed line to the relaxed muscle. The absence of the activation dynamics means that the roll-off at high frequencies is only -40 dB/decade. At lower frequencies (below about 20 rad/s), the responses are similar to those of the muscle and steering system with activation dynamics.

2.4. *Stretch reflex*

So far in this paper, muscle activation has been considered to come from the alpha motor neurons in the spine. The alpha motor neurons receive signals from two main sources. Signals can be sent directly from the motor cortex in the brain; in Figure 1 this signal is labelled α. In addition, the alpha motor neurons can be signalled by reflex action, which is predominantly a closed-loop feedback control of muscle length known as the stretch reflex. Gamma motor neurons in the spine activate special fibres in the muscle called spindles. The motor neurons are believed to adjust the length of the spindles according to the muscle length (or handwheel angle) expected by the brain. If the muscle length differs from the expected length, the spindles are strained and send a signal to the alpha motor neurons, which in turn activate the muscle to achieve the expected muscle length. The function of the muscle spindles is represented in Figure 1 by the summation circle, which calculates the difference between the expected angle γ and the actual angle θ. The difference is then operated upon by a reflex gain (H_r) and a delay (D_r) before activating the muscle via the alpha motor neuron. In the present investigation, the reflex gain is set to 0 or 50 Nm/rad, guided by the measurements in [9]. The reflex delay is largely a function of neural conduction velocities and the distance of the muscle from the motor neurons in the spine; the delay is set to 40 ms for tensed and relaxed conditions [11].

The stretch reflex system is a subject of ongoing research in the neuroscience field, for example [23], and there is at present incomplete understanding about its role in human motor control. The stretch reflex model presented in this paper is likely to be highly simplified, but can be regarded as representative of first-order effects. In practice, stretch reflex is known to have short-latency and long-latency components, the latter thought to be actively programmable by the brain. The reflex action is also thought to be sensitive to muscle velocity and force, as well as muscle displacement.

Figure 7(b) shows the transfer functions of the muscle and steering system with the addition of the stretch reflex loop. The γ activation signal is zero. In comparison to the transfer functions of the tensed muscle and steering system without reflex shown in Figure 7(a), the low frequency magnitudes are smaller because the stretch reflex loop provides muscle stiffness at frequencies down to zero. However, the stretch reflex loop also results in a lightly damped resonance at about 10 rad/s, the properties of which are strongly influenced by the reflex gain H_r and delay D_r. The frequency of the resonance increases with the gain and the damping ratio tends to reduce as the delay and gain increase [10]. At frequencies above the resonance, the response is similar to the system without the stretch reflex loop, Figure 7(a).

2.5. *Muscle, steering, stretch reflex and vehicle*

Next the steering–muscle–reflex system (H_s, H_a, H_b, H_r and D_r) is connected to the vehicle (H_v). The vehicle is travelling at constant speed $U = 30$ m/s. Lateral tyre forces at the front axle are fed back to the pinion/handwheel via the torque T_v. The trail distance is $d = 75$ mm. There is no closed-loop path following at this stage and thus there is no central activation of

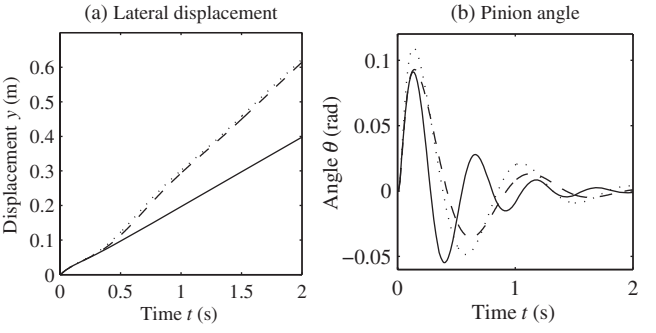

Figure 8. Lateral displacement and pinion angle response to impulsive disturbance in F_d for the muscle, steering, reflex and vehicle model, in tensed + reflex (solid), tensed (dashed) and relaxed (dotted) conditions.

the muscle ($\alpha = 0$ and $\gamma = 0$). Using this model, the effect of steering torque feedback arising from disturbances on the vehicle can be investigated.

Figure 8(a) shows the vehicle lateral displacement response y to a lateral force impulse of 500 Ns at the centre of mass (F_d), for tensed muscles with 50 kN/m reflex gain (solid), tensed without reflex (dashed) and relaxed without reflex (dotted). In all three cases, the pinion angle response is such that it causes the vehicle to gain steady velocity in the direction of the impulse disturbance. The global lateral velocity $\dot{y}$ is least for the tensed with reflex condition. This is because the reflex loop stiffens the steering's response to lateral tyre forces and thus reduces the amplitude of the pinion angle response. There is little difference in the response with tensed and relaxed muscles without reflex. This is consistent with the corresponding frequency responses in Figure 7(a).

Note that for the case of no torque feedback ($d = 0$ m), the muscle and steering system is not excited and thus the vehicle response is the same as shown in Figure 4(a) and independent of the muscle and reflex condition. In Figure 4(a), the eventual steady global lateral velocity $\dot{y}$ of the vehicle was zero thus the torque feedback in combination with the steering and the muscle response can be regarded as having a deleterious effect on the response of the vehicle to lateral disturbances at the centre of mass.

The simulations were repeated for 500 Ns impulsive disturbances at the front and rear axle positions (F_f and F_r). Figure 9 shows the resulting steady-state global lateral velocity responses ($\dot{y}$). In the first group of three bars (1 on the horizontal axis), the results for the vehicle with fixed steering are shown, these velocities corresponding to those observed in Figure 4(a). If the steering is now free to steer, but the driver does not hold the steering wheel, the velocities shown in the second group of three bars (2) are obtained; the action of the lateral front tyre force acting on the steering mechanism results in a non-zero velocity response to F_d compared with the fixed steering case. If the driver now holds onto the steering wheel, either tensed or relaxed, but with no reflex action, the third and fourth groups of bars (3 and 4) are derived; it can be seen that the velocities are very similar to the hands-free case (2). This is because the response is determined mainly by the passive properties of the steering, which dominate over the tensed or relaxed muscles. In the final group of bars (5), the stretch reflex is included with the tensed muscle condition. The velocities for impulses applied at the front and rear of the car increase significantly compared with the no reflex cases (2–4), but the response to impulse at the centre of the vehicle decreases, as observed in the solid line of Figure 8(a). This is because the reflex action stiffens the arms and reduces the pinion angle response compared with the no reflex cases (2–4). The vehicle response thus tends towards that of the fixed steering case (1) where the pinion angle response was zero. Thus, the addition of reflex action can be seen

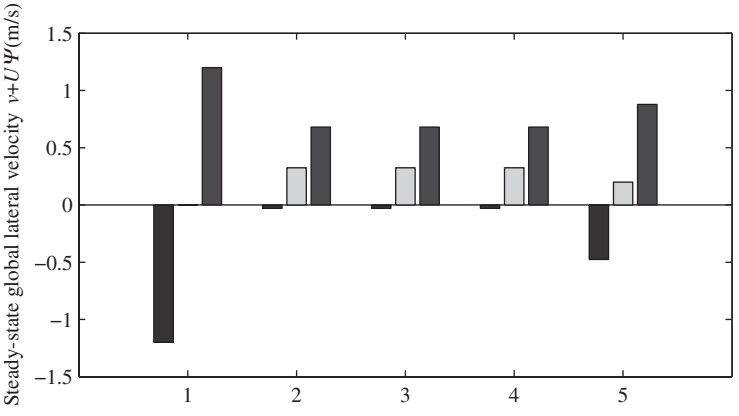

Figure 9. Steady-state global lateral velocities after lateral force impulse on the muscle, steering, reflex and vehicle model. Left-hand bar F_r, middle bar F_d, right-hand bar F_f. 1, fixed steering; 2, hands-free steering; 3, tensed without reflex; 4, relaxed without reflex and 5, tensed with reflex.

to either increase or decrease the magnitude of the steady-state global lateral velocity of the vehicle, depending on where the disturbance is applied to the vehicle.

2.6. *Summary*

A driver–vehicle model was assembled with the steering torque feedback and neuromuscular dynamics, including stretch reflex (Figure 1), but initially without path-following control. The effect of tensing (co-contracting) the muscles was seen to increase the damping of the arms (Figure 6). The stretch reflex gain was seen to increase the stiffness of the arms and introduces a lightly damped resonance (Figure 7). Lateral impulsive disturbances on the vehicle resulted in excitation of the neuromuscular and steering system, leading to modification of the vehicle's directional response to the disturbance (Figure 9). Changing the intrinsic muscle properties by tensing or relaxing the muscles made little difference to the directional response, but the stiffening effect of the reflex action had a significant effect (Figure 9). The effect of the reflex action depended on the longitudinal position of the disturbance; the disturbance position affects the magnitude and direction of the excitation of the neuromuscular and steering system (Figure 4). The results are based on a 'first-order' model of the neuromuscular system effects. It should be noted that there is incomplete knowledge in the field of motor neuroscience research regarding: how a human chooses to co-contract muscles; how reflex action depends on the state of the muscles and how reflex properties are modified consciously. In Section 3, a path-following controller is added to the model.

3. Path following

In this section, the generation of activation signals α and γ by the brain to achieve the path-following control is considered. The relevant blocks in Figure 1 are K, D_c and H_f.

3.1. *Control*

Block D_c in Figure 1 is a cognitive time delay which represents the information processing delay of the brain and the time taken for signals to travel from the sensory organs and to the motor neurons. In practice, the various sensory channels differ in their time delay and

frequency response; in the present work, it is assumed that the system states are measured perfectly and that a single value of time delay applies. The time delay is implemented as a discrete-time shift-register [24] and is set to $t_c = 0.5$ s.

Block H_f is a forward model of the delay-muscle–steering–vehicle system (D_c, H_a, H_b, H_s, H_v). The forward model allows the pinion angle θ response to a (pre-delay) activation signal α_K to be calculated. The expected angle is the γ signal sent to the reflex system (H_r and D_r). If the forward model H_f is correct, and if there are no unexpected disturbances on the muscle–steering–vehicle system, then the expected angle γ exactly matches the true angle θ and no reflex action occurs. The use of a forward model is an improvement over earlier driver–vehicle models [10,16,17] that used an inverse model with associated complication to ensure a proper transfer function.

The pre-delay activation signal α_K is generated by control gains in block K acting upon the previewed lateral displacements y_j of the road path and upon the states x of the system ($D_c, H_f, H_r, D_r, H_a, H_b, H_s, H_v$). Preview of the road path is modelled by a discrete-time shift-register acting upon the road path lateral displacement y_p at the end of the prediction horizon $t_p = 3$ s ahead of the vehicle. The control gains K can be obtained using a discrete-time linear quadratic regulator or linear model predictive control formulation [15,24,25]. The formulation involves a cost function J to be minimised, comprising the weighted sum of mean square values of the lateral path-following error, time integral of the lateral path-following error and the α_K activation signal:

$$J = \sum_j q_1 y_{\text{error}}(j)^2 + q_2 y_{\text{integral}}(j)^2 + \alpha_K(j)^2, \tag{6}$$

where j is the prediction time-step index; q_1 a weighting on the lateral displacement y_{error} of the vehicle from the target path; q_2 a weighting on the time integral of the lateral displacement y_{integral} of the vehicle from the target path. Note that the cost function does not account for the muscle activation required to maintain the tensed condition. A detailed review and description of the procedure for defining the previewed road path and for calculating the optimal control gains K can be found in [15]. Default values for the cost function weights are given in Table 1. An alternative formulation of the cost function was proposed in [12] which attempts to account for muscle activation arising from α and γ signals.

3.2. *Response*

3.2.1. *Road path displacement input*

Figure 10 shows the frequency response from path displacement y_p to vehicle global lateral displacement y. The solid line and dash-dot line correspond to the tensed and relaxed muscle conditions with the steering torque feedback ($d = 75$ mm). The dashed line and the dotted line correspond to the tensed and relaxed muscle conditions without the steering torque feedback ($d = 0$ mm). At frequencies of about 8 rad/s and below the gain is unity, which means that the vehicle follows the path with negligible error. It can be seen that the muscle condition and feedback condition make little difference to the response bandwidth. The relaxed condition has very slightly higher bandwidth than the tensed condition, due to the slightly lower arm inertia in the relaxed condition.

Only when the cost function weights on the path error and integral error are significantly decreased does a difference emerge. As these weights are decreased, the muscle activation is decreased and the bandwidth decreases. If the weights are decreased by a factor of 10^6, the bandwidth of the no feedback condition reduces to about 1.0 rad/s and the bandwidth of the feedback condition reduces to about 0.5 rad/s (Figure 11). This lower bandwidth for the

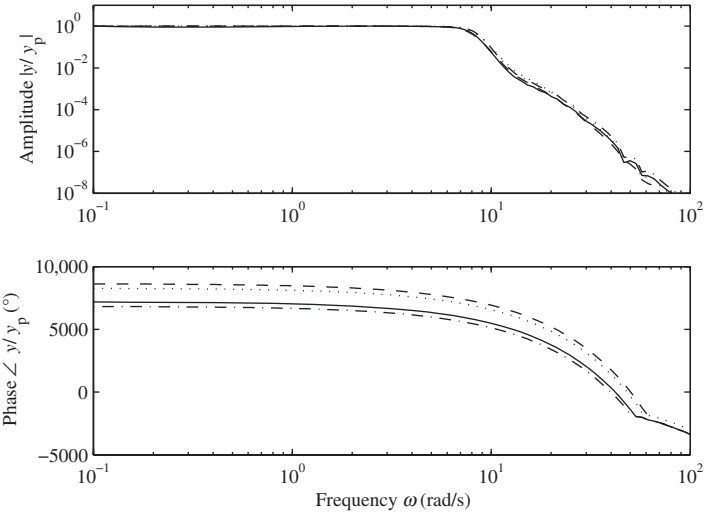

Figure 10. Frequency responses of path-following controller for tensed + feedback (solid), relaxed + feedback (dashed), tensed no feedback (dash-dot) and relaxed no feedback (dotted).

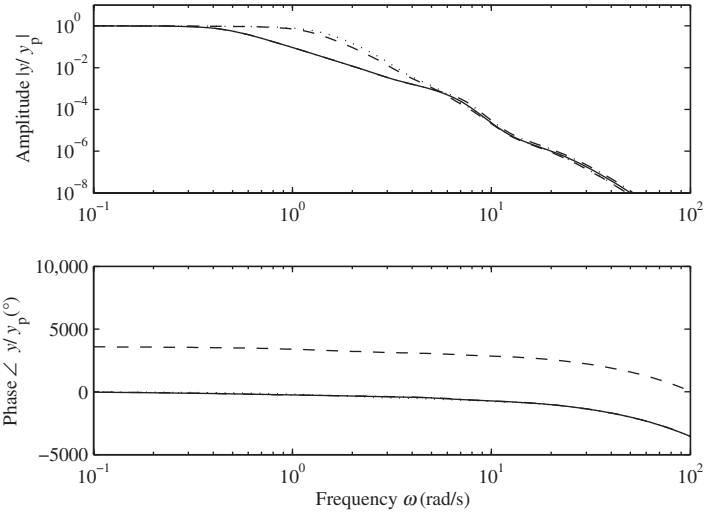

Figure 11. Frequency responses of path-following controller for tensed + feedback (solid), relaxed + feedback (dashed), tensed no feedback (dash-dot) and relaxed no feedback (dotted). Cost function weights $q_1 = q_2 = 0.1$.

feedback case is a consequence of the cost function. When the steering torque feedback is included, some muscle activation is required to react to the feedback torque; to minimise the cost function, the controller reduces the path-following accuracy, leading to reduced bandwidth. When the weights on the path error are much higher (as in Figure 10), the muscle activation plays a smaller part in the cost function and thus the difference in bandwidth due to the feedback condition is small. Irrespective of the cost function weights, the muscle condition (tensed or relaxed) appears to have little influence on the path-following control bandwidth, which is consistent with the observations in Figure 9.

The cognitive delay D_c has little effect on the transfer functions because the controller can compensate by looking further along the previewed road path, as noted in [24,26]. Again,

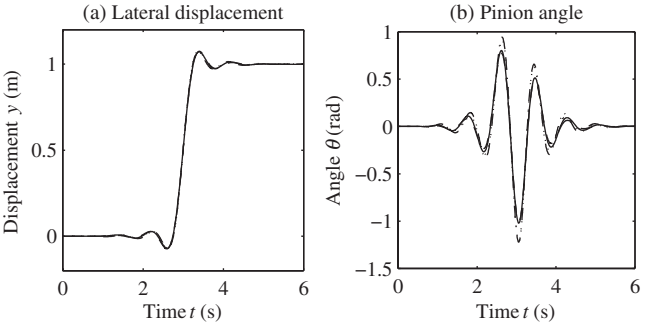

Figure 12. Lateral displacement and pinion angle response to a unit step in road path lateral displacement at $t = 3$ s, for tensed + feedback (solid), relaxed + feedback (dashed), tensed no feedback (dash-dot) and relaxed no feedback (dotted). Path-following controller enabled.

note that the cost function does not account for the muscle activation required to maintain the tensed condition; see [10] for some analysis of this aspect.

The stretch reflex has no effect on the frequency responses because there are no unexpected disturbances. The road path displacement is previewed by the controller and the pinion angle response matches exactly the response predicted by the forward model. Thus, the reflex case is not shown explicitly in Figure 10.

Lateral displacement and pinion angle response histories for a unit step in the road path lateral displacement are shown in Figure 12 for the higher cost function weights. The step occurs at a time of 3 s. The steering action begins at about 1 s, which is 2 s before the vehicle reaches the step in the road path, confirming the preview action of the controller. The similarity of the responses across the various conditions is consistent with the frequency responses shown in Figure 10.

3.2.2. *Lateral force disturbance input*

The frequency response of the system from the lateral force disturbance input at the centre of mass (F_d) to the lateral displacement output y is shown in Figure 13. There are six lines on the graph. The upper three lines (black) correspond to tensed (solid), relaxed (dashed) and tensed plus reflex (dash-dot) conditions all with steering feedback. The tensed and relaxed lines essentially lie on the top of each other, and the tensed plus reflex line (dash-dot) has slightly lower gain at frequencies up to about 10 rad/s; the reflex stiffens the arms and thus the steering angle response to the steering torque feedback reduces, reducing the lateral displacement response y.

The lower three lines (grey) in Figure 13 are without steering feedback. The three lines are essentially the same as each other. The tensed (solid) and tensed plus reflex (dash-dot) lie on the top of each other because the reflex action has no effect when there is no steering feedback. The relaxed case only differs very slightly from the tensed case in the region of 5 rad/s, arising from the differences seen in Figure 7. The gains are lower than for the systems with feedback at frequencies below about 10 rad/s because there is no deleterious steering response arising from the feedback.

The general trend for the gains to reduce as frequency reduces below about 2 rad/s demonstrates the effectiveness of the path-following controller in minimising the path-following error. Lower values of cost function weights increase the maximum magnitude of the transfer functions and increase the difference in performance between the feedback and no feedback cases, for the reasons noted in Section 3.2.1.

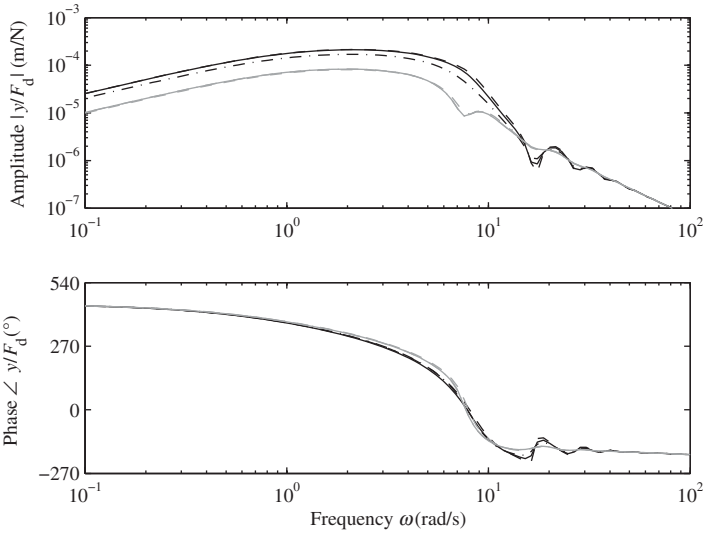

Figure 13. Frequency response of lateral displacement y to F_d disturbance for tensed (solid), relaxed (dash) and tensed + reflex (dash-dot) conditions. Upper three lines (black) are with steering feedback, lower three lines (grey) are without. Path-following controller enabled.

Time histories of lateral displacement y when a 500 Ns impulse is applied at the centre of the vehicle are shown in Figure 14(a). There are six lines on the graph. The three lines with larger displacement (black) correspond to tensed (solid), relaxed (dashed) and tensed plus reflex (dash-dot) conditions all with steering feedback. The effect of the path-following control is evident in the displacement eventually returning to zero, in contrast to the responses without path-following control shown in Figure 8(a). The smaller amplitude lines in Figure 14(a) (grey, laying on top of each other) are for no steering feedback. The corresponding pinion wheel angle responses are shown in Figure 14(b).

The effect of the cognitive delay is now apparent. There is no preview of the force disturbance and thus the path-following control takes no action until the delay time t_c has passed. This is evident in Figure 14(b) for the three lines without feedback (grey); there is no driver response until the cognitive delay has passed. The graph shows zero pinion angle θ until $t > 0.5$ s. With steering torque feedback, the driver response from $t = 0$ to 0.5 s arises from the passive and reflex behaviour of the neuromuscular system.

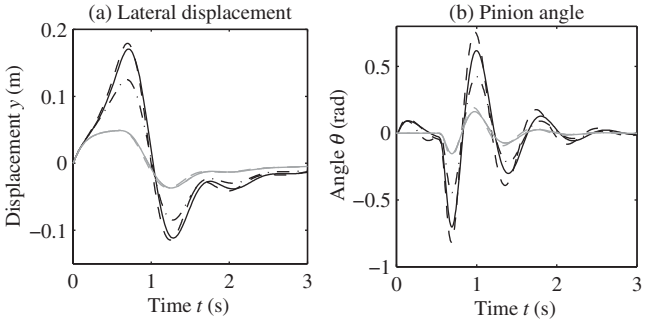

Figure 14. Lateral displacement and pinion angle response to impulsive disturbance in F_d at $t = 0$ s for tensed (solid), relaxed (dash) and tensed + reflex (dash-dot) conditions. The three larger amplitude responses (black) are with steering feedback, the three lower amplitude responses (grey) are without. Path-following controller enabled.

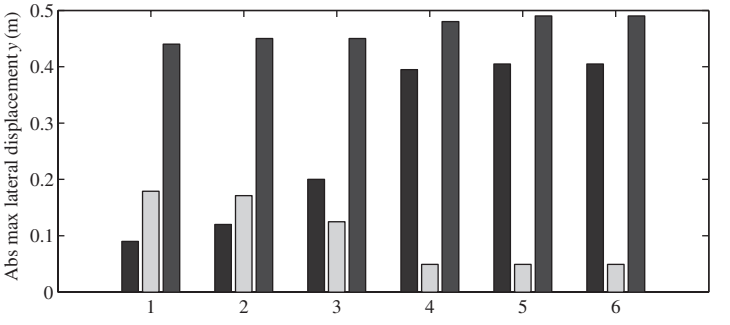

Figure 15. Maximum lateral displacements after lateral force impulse. Left-hand bar F_r, middle bar F_d, right-hand bar F_f. 1–3 with feedback, 4–6 without feedback. 1,4, relaxed without reflex; 2,5, tensed without reflex; 3,6, tensed with reflex. Path-following controller enabled.

The maximum lateral displacements y are shown in Figure 15. There are six groups of three bars. Within each group, the three bars correspond to impulses applied at the rear (F_r), middle (F_d) and front (F_f) of the vehicle. The first three groups of bars correspond to relaxed (1), tensed (2) and tensed plus reflex (3) conditions for the system with steering feedback. The second three groups (4–6) correspond to the same muscle conditions but without steering feedback. In all cases, the final value of the path displacement is zero as a result of integral action in the path-following controller.

When there is no steering feedback, the relaxed (4), tensed (5) and tensed plus reflex (6) conditions all give similar maximum displacements to each other, as expected from the frequency responses in Figure 13. The displacement magnitudes are smallest when the force disturbance is applied to the centre of the car, and approximately equal to the displacement of 50 mm achieved by the open-loop vehicle (Figure 4). In the first 0.5 s (before the path-following controller begins to act), the vehicle with no steering feedback responds as if there was no driver present and thus the lateral vehicle displacement arising from the impulse in F_d corresponds to that seen in Figure 4. The displacement magnitudes achieved when the impulse is applied to the front or rear of the vehicle are about 0.4–0.5 m and are strongly dependent on the cognitive delay. If the delay is increased, the vehicle displaces further away from the target path before the path-following controller takes action to return the vehicle to the target path (not shown).

The results for the systems with steering feedback are a little more complicated. Considering the impulse applied to the centre of the vehicle (middle bars of 1–3), the displacement is larger than the no feedback case (middle bars of 4–6). This is consistent with the steering feedback causing a pinion response that steers the vehicle away from the target path. The vehicle is then returned to the straight path by the path-following controller. The reflex action acts to reduce the pinion response to steering feedback and thus the lateral vehicle displacement (middle bar, 3) is less than without reflex action (middle bars of 1 and 2). These results are consistent with the steady-state lateral velocities arising when the path-following controller is absent (Figure 9). The displacement magnitudes arising from impulses at the front (F_f, left-hand bar of 1–3) and rear (F_r, right-hand bar of 1–3) of the vehicle can similarly be understood by referring to Figure 9.

3.3. *Summary*

A path-following controller was implemented, including a cognitive time delay and a forward model for generation of the reflex demand signal. A cost function allowed the trade-off between

path-following accuracy and control activity to be set. An integral of the path error term in the cost function allowed steady-state path-following errors to be eliminated. The lateral path displacement to lateral vehicle displacement transfer function (Figure 10) showed that there was little difference in path-following bandwidth for the vehicles with and without steering torque feedback when the cost function placed emphasis on minimising path error. However, when emphasis was placed on minimising control activity, the steering torque feedback caused the bandwidth to reduce compared with the no feedback case. The relaxed and tensed muscle conditions made little difference to the bandwidth. Reflex gain and cognitive delay had no effect because the lateral path displacement was previewed. The lateral vehicle displacement response of the vehicle to lateral force impulse on the vehicle was strongly dependent on: the longitudinal position of the impulse; the amount of steering torque feedback (d); cognitive time delay; and reflex gain (Figure 15). Again, the tensed or relaxed muscle condition (intrinsic muscle properties) had little effect.

4. Torque overlay and angle overlay

The introduction of steering technology that assists the driver in controlling the vehicle by adding a torque and/or an angle to the pinion (torque overlay and angle overlay) raises the question of the influence of the neuromuscular system. Figure 16 shows how the steering model of Figure 5 is modified to allow angle overlay and torque overlay inputs. The inertia of the steering system I_s is split into two parts I_{hw} and I_{pinion} between which a relative angular displacement $\theta_{overlay}$ can be specified. The handwheel angle is then $\theta_{hw} = \theta + \theta_{overlay}$. The angle overlay is generated in the model by connecting a very stiff spring $k_o = 1$ MNm/rad

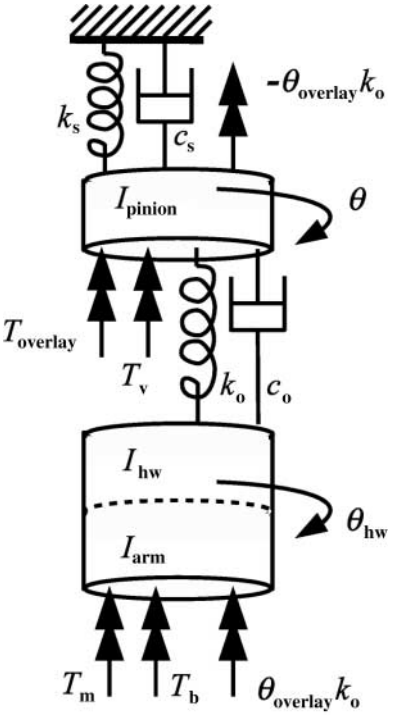

Figure 16. Torque overlay and angle overlay model with two rotational degrees of freedom.

between the inertias and then applying equal and opposite torques to the inertias, the torque being the desired overlay angle θ_{overlay} times the stiffness k_{o}. A parallel torsional damper $c_{\text{o}} = 1$ kNm/rad/s reduces resonance. A torque overlay can be specified as a torque T_{overlay} applied between the pinion and vehicle ground. The equations of motion are as follows:

$$(I_{\text{arm}} + I_{\text{hw}})\ddot{\theta}_{\text{hw}} + c_{\text{o}}(\dot{\theta}_{\text{hw}} - \dot{\theta}) + k_{\text{o}}(\theta_{\text{hw}} - \theta) = T_{\text{m}} + T_{\text{b}} + k_{\text{o}}\theta_{\text{overlay}}, \tag{7}$$

$$I_{\text{pinion}}\ddot{\theta} + c_{\text{o}}(\dot{\theta} - \dot{\theta}_{\text{hw}}) + k_{\text{o}}(\theta - \theta_{\text{hw}}) = T_{\text{overlay}} + T_{\text{v}} - k_{\text{o}}\theta_{\text{overlay}}. \tag{8}$$

4.1. *Torque overlay*

Figure 17 shows the frequency response of the vehicle lateral displacement to torque overlay disturbance. The path-following controller is enabled. The magnitude of the transfer functions is generally greater without steering feedback. This is because the angular response of the steering is reduced when the torque overlay has to react the steering torque feedback. The relaxed muscle condition gives slightly higher gain than the tensed condition. Adding reflex to the tensed condition reduces the gain, because the reflex stiffens the arm's response to the torque overlay.

Figure 18(a) shows the vehicle path time response to a unit step in torque overlay. The path-following controller is enabled. The amplitude of the vehicle lateral displacements is consistent with the observed features of the transfer functions. The maximum displacement is about 0.3 m at 1 s, for the relaxed condition without reflex and without steering feedback. The corresponding handwheel angle responses are given in Figure 18(b). For the no reflex conditions (solid and dashed lines), the angle increases for the first 0.5 s are in a direction that causes the vehicle lateral displacement to increase. After 0.5 s, the path-following controller acts and the handwheel angle moves in the opposite direction in order to reduce the lateral displacement to zero. The addition of reflex action to the tensed condition (dash-dot line) acts to bring the handwheel angle back towards zero before the path-following controller comes into play, thus reducing the corrective steering action required of the path-following controller.

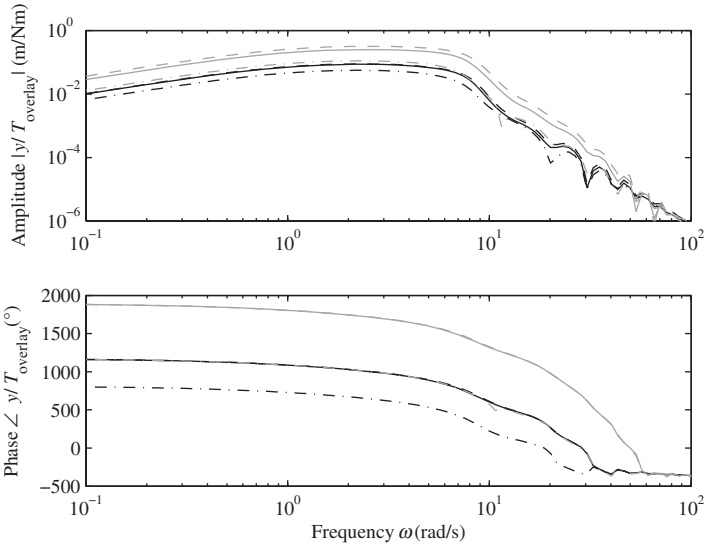

Figure 17. Frequency response of lateral displacement y to T_{overlay} disturbance for tensed (solid), relaxed (dash) and tensed + reflex (dash-dot) conditions. Lower three lines (black) are with steering feedback, upper three lines (grey) are without. Path-following controller enabled.

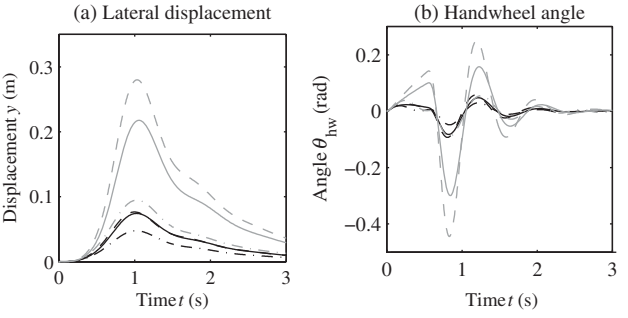

Figure 18. Lateral displacement and handwheel angle response to unit step in T_{overlay} at $t = 0$ s for tensed (solid), relaxed (dash) and tensed + reflex (dash-dot) conditions. The three lower amplitude responses (black) are with steering feedback, the three larger amplitude responses (grey) are without. Path-following controller enabled.

The response of the driver model to a step in torque overlay raises a question about the forward model H_{f} used to calculate the gamma signal γ. The forward model has no knowledge of external disturbances on the vehicle. For a step in torque overlay, it is reasonable to assume that the human driver would eventually identify the presence of the torque and make an appropriate adjustment to the α and γ signals. The steady-state condition after the occurrence of the step in torque overlay would likely involve a non-zero α signal to react to the torque overlay and a zero γ signal to avoid permanent activation of the reflex system with the steer angle at zero. In the present model structure, the γ signal remains finite and the α signal is increased to react both the torque overlay and the torque arising from the reflex action. Nevertheless, the steady-state path-following error is zero, aided by the integral term in the cost function. Droogendijk [16] identified the same issue regarding external disturbances and incorporated a hypothetical correction torque in his driver model.

As previously discussed, the operation of the reflex system remains an area of active research in the neuroscience field. The way in which the alpha–gamma signals and the reflex gains are adjusted to deal with unexpected disturbances on the vehicle remains an open question. One might expect the driver's internal model to be updated to account for external disturbances. In the event that the disturbance is constant as in the case of the step in torque overlay, it would seem straightforward for the driver to make the appropriate corrections to the alpha–gamma signals. But in a more general case of random and therefore unpredictable disturbances, it seems likely that the driver might adjust the reflex gains and muscle co-contraction according to the expected nature of the disturbances, in the manner of a robust controller. In the example of lateral impulses on the vehicle, the reflexes might be adjusted according to the expected longitudinal position of the disturbance, in order to avoid reflex responses that reinforce the effect of the disturbance (Figure 15). This is an area for further study.

4.2. *Angle overlay*

Figure 19 shows the frequency response of vehicle lateral displacement to angle overlay θ_{overlay} disturbance. The path-following controller is enabled. As in the case of torque overlay, the gain is higher without the steering torque feedback. The gain tends to increase as the muscles move from relaxed to tensed to tensed with reflex, whereas the opposite trend is apparent in the torque overlay case, Figure 18. For angle overlay to have a big effect on the lateral displacement, it is necessary for the arm displacement to be small, so that the overlay appears at the pinion and not at the handwheel. Reflex tends to maintain the handwheel angle θ_{hw} close

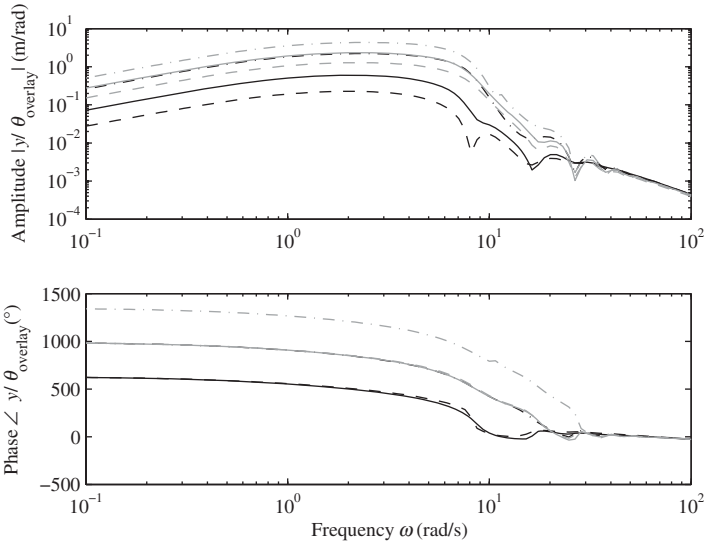

Figure 19. Frequency response of lateral displacement y to θ_{overlay} disturbance for tensed (solid), relaxed (dash) and tensed + reflex (dash-dot) conditions. Lower three lines (black) are with steering feedback, upper three lines (grey) are without. Path-following controller enabled.

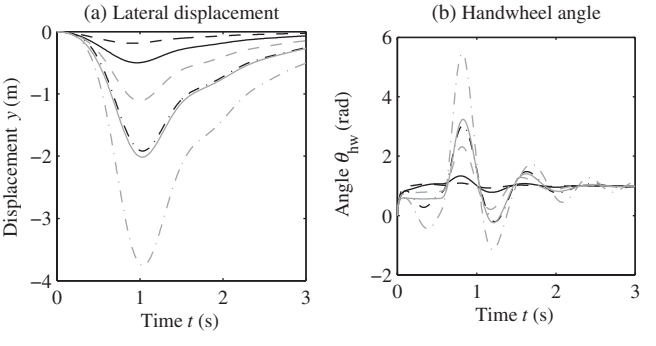

Figure 20. Lateral displacement y and handwheel angle θ_{hw} response to unit step in θ_{overlay} for tensed (solid), relaxed (dash) and tensed + reflex (dash-dot) conditions. The three smaller amplitude responses (black) are with the steering torque feedback, the three larger amplitude responses (grey) are without. Path-following controller enabled.

to zero and thus the overlay angle θ_{overlay} appears mainly at the pinion, leading to large lateral displacements.

Figure 20(a) shows the vehicle lateral displacement time response to a unit step in angle overlay θ_{overlay}. The path-following controller is enabled. The amplitude of the vehicle lateral displacements is consistent with the observed features of the transfer functions. The maximum displacement is about 3.8 m at 1 s, for the tensed condition with reflex and without steering feedback. The corresponding handwheel angle θ_{hw} responses are given in Figure 18(b).

For the tensed condition with reflex (dash-dot lines), the handwheel angle θ_{hw} reaches to about 0.5 rad in the few milliseconds following the application of the overlay angle θ_{overlay}. The pinion angle θ response is not shown, but because $\theta = \theta_{\text{hw}} - \theta_{\text{overlay}}$, it can be deduced that the pinion rotates by about 0.5 rad in the opposite direction to the handwheel. Shortly, after the overlay angle θ_{overlay} is applied, the handwheel angle θ_{hw} heads towards the straightahead, 0 rad position. This happens well within 0.5 s and thus can be ascribed to the passive and reflex

dynamics of the arms. From about 0.5 s, the handwheel angle θ_{hw} begins moving to a final value of 1 rad, which is the angle required to oppose the angle overlay $\theta_{overlay}$ and thus maintains the straight path following. This action can be ascribed to the cognitive path-following control.

For the no reflex conditions (solid and dashed lines) and no steering feedback, the handwheel angle θ_{hw} follows the overlay angle $\theta_{overlay}$ quite closely, and thus the pinion angle θ remains close to the 0 rad required for straight path following. The path-following control comes in at 0.5 s to pull the handwheel angle θ_{hw} into a final value of 1 rad. It is clear that the reflex action described in the preceding paragraph is not helping the driver to maintain a straight path because it acts to keep the handwheel angle θ_{hw} at 0 rad, whereas an angle of 1 rad is ultimately required to compensate for the 1 rad overlay angle.

5. Experiments

A fixed-base driving simulator was used to collect data for preliminary validation of the model. The experiment and initial data analysis were performed by Sardar [27]. The simulator comprised: a real-time linear lateral–yaw vehicle model; the torque-feedback steering wheel used by Hoult [11]; and a visual display of the target road path as viewed from the simulated moving vehicle. Vehicle parameter values were similar, but not identical, to those used in generating the simulation results in this paper. The steering torque feedback (d) was set to zero. The simulator has also been used by Kim [2], Odhams [14,13] and Pick [10].

The experiment involved the test subject guiding the vehicle at constant speed along a straight target path. At a random time a step angle overlay of 3°, 6° or 9° was introduced without warning. The driver was required to apply steering action to follow the straight target path. In advance of the overlay occurring, the driver either tensed (co-contracted) or relaxed their arm muscles, as instructed by a message on the display. Each test subject was presented with 18 events (three amplitudes $\times$ two muscle conditions $\times$ three repeats). The presentation order of the angle amplitude and muscle condition combinations was randomised to minimise the anticipatory response. In addition, the direction of the angle overlay was randomised. Five test subjects completed the experiment. Each test subject completed a number of familiarisation events before the definitive data were collected.

Figure 21(a) shows the nine handwheel angle responses and their mean from one test subject in the tensed muscle condition. The responses resulting from the positive and negative overlay angles have been normalised to one direction. The responses from 3° and 9° overlay angles have been multiplied by 2 and 2/3, respectively, to normalise to the 6° overlay angle (Sardar [27] showed that responses scaled approximately linearly with the overlay angle amplitude). A significant variance in response is noticeable. Note that the mean response does not necessarily represent a typical response. Looking at the mean response, at 1 s the angle overlay is applied and the handwheel angle quickly reaches 2–3°. The pinion angle response is not shown, but because the pinion angle $\theta = \theta_{hw} - \theta_{overlay}$, it can be deduced that the pinion angle rotates in the opposite direction by 3–4°. Shortly after the overlay angle is applied the handwheel angle returns back to the straight ahead position and then to about -3° to -4°. This happens well within 0.5 s of the angle overlay and thus can be ascribed to the passive dynamics of the arms and reflex action. From about 0.4 s, the handwheel angle begins its move to a mean level of 6°, which is the angle required to oppose the angle overlay and maintain straight path following. This action can be ascribed to the cognitive path-following control of the test subject. In comparison to the simulated behaviour for the tensed condition with reflex and no feedback (grey dash-dot) shown in Figure 20(b), there is generally good agreement, although the cognitive control action has lower amplitude and longer duration in the measured data.

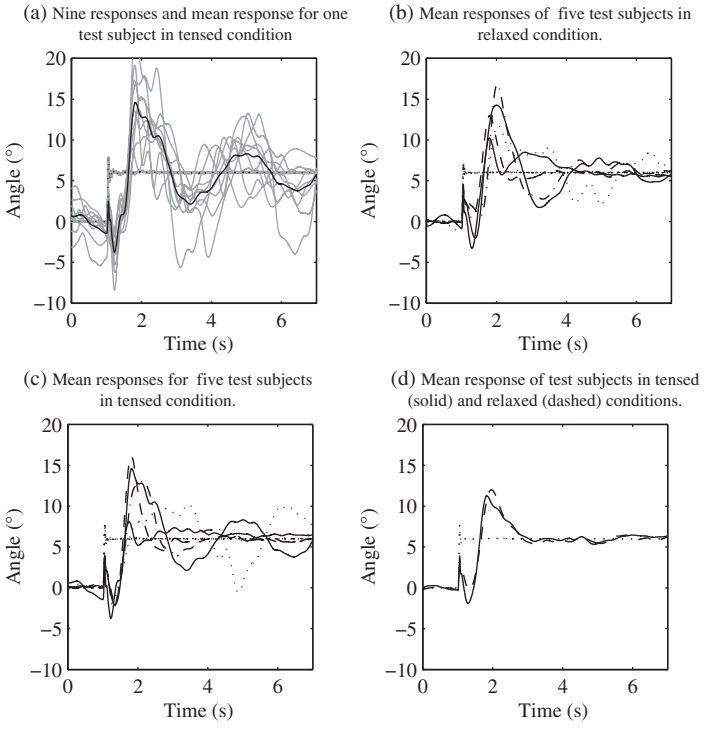

Figure 21. Measured handwheel angle responses and step overlay angle against time [27].

Figure 21(b) shows the mean handwheel angle responses of five test subjects in the relaxed muscle condition and Figure 21(c) shows the mean responses of five test subjects in the tensed muscle condition. Both figures show inter-subject variability, particularly in the cognitive control phase. Figure 21(d) shows the mean response of the five test subjects, for the tensed (solid line) and for the relaxed (dashed line) conditions. The results suggest that there is significant reflex response in both the tensed and relaxed conditions, although the tensed condition shows a stronger response than the relaxed condition (the handwheel angle drops to about -2° compared with 0°). If there were no reflex responses, the handwheel angle would likely initially follow the overlay angle quite closely, as predicted in Figure 20(b), grey solid or dashed line.

6. Conclusion and further work

A driver–vehicle model was assembled with steering torque feedback and neuromuscular dynamics, including stretch reflex, but initially without path-following control. The effect of tensing (co-contracting) the muscles was modelled according to experimentally identified behaviour, which showed an increase in the intrinsic damping of the arms. The stretch reflex gain in the model had the effect of increasing the stiffness of the arms and introducing a lightly damped resonance.

Lateral impulsive disturbances on the vehicle with steering torque feedback resulted in excitation of the neuromuscular and steering system, leading to modification of the vehicle's directional response to the disturbance. Tensing or relaxing the muscles (modifying the intrinsic properties) made little difference to the directional response, but the stiffening effect

of the reflex action had a significant effect, dependent on the longitudinal position of the disturbance.

A path-following controller was implemented, including a cognitive time delay and a forward model for generation of the reflex demand (gamma) signal. A cost function allowed the trade-off between path-following accuracy and control activity to be set. The transfer function from lateral road path displacement to lateral vehicle displacement showed that there was little difference in path-following bandwidth for the vehicles with and without steering torque feedback when the cost function placed emphasis on minimising path error. However, when emphasis was placed on minimising control activity, the steering torque feedback caused the bandwidth to reduce compared to the no feedback case. The relaxed and tensed muscle conditions made little difference to the path-following bandwidth. Reflex gain and cognitive delay had no effect because the lateral path displacement was previewed. The lateral displacement response of the vehicle to the lateral force impulse on the vehicle was strongly dependent on: the longitudinal position of the impulse; amount of steering torque feedback; cognitive time delay; and reflex gain.

The model with path-following control was extended to include angle and torque overlay functions. Steering torque feedback reduced the disturbing effect of torque overlay and angle overlay inputs. Reflex action reduced the disturbing effect of a torque overlay input but increased the disturbing effect of an angle overlay input. Experiments on a driving simulator showed that measured handwheel angle response to a step angle overlay input was consistent with the response predicted by the model with reflex action. However, there was significant intra- and inter-subject variability.

The results highlight the significance of the driver's neuromuscular dynamics and the steering system dynamics in determining the vehicle response to disturbances. The model is thought to provide a suitable basis for investigating torque and angle overlay strategies that account for passive and reflex behaviour of a driver's arms. However, further work is planned to obtain a more complete understanding of the effects. In particular, the following questions need to be addressed: how does a driver decide on the muscle co-contraction level? How does reflex action depend on the state of the muscles? To what extent does a driver consciously modify the reflex properties? How are the alpha–gamma signals controlled in the presence of input and parameter uncertainties? What determines the random component of driver response?

Acknowledgements

The author wishes to thank Dr Andrew Pick, Dr Andrew Odhams, Dr Will Hoult and William Sardar, who are past members of the Driver–Vehicle Dynamics Research Group at Cambridge University Engineering Department.

References

[1] Available at www.vehicledynamics.org.
[2] N. Kim and D.J. Cole, *A model of driver steering control incorporating the driver's sensing of steering torque*, Veh. Syst. Dyn., first published on 03 March 2011 (iFirst).
[3] N. Kim and D.J. Cole, *A Multiple-Model Predictive Control Approach to Modelling Driver Steering Torque Feedback*, Proceedings of 21st IAVSD Symposium on Dynamics of Vehicles on Roads and Tracks Stockholm, 2009.
[4] A. Modjtahedzadeh and R.A. Hess, *A model of driver steering control behaviour for use in assessing vehicle handling qualities*, ASME J. Dyn. Syst. Meas. Control 115 (1993), pp. 456–464.
[5] A.J. Pick and D.J. Cole, *Neuromuscular dynamics and the vehicle steering task*, Suppl. Veh. Syst. Dyn. 41 (2004), pp. 182–191.
[6] A.J. Pick and D.J. Cole, *Neuromuscular dynamics in the driver–vehicle system*, Suppl. Veh. Syst. Dyn. 44 (2006), pp. 624–631.

[7] A.J. Pick and D.J. Cole, *Measurement of driver steering torque using electromyography*, Trans. ASME J. Dyn. Syst. Meas. Control 128 (2006), pp. 960–968.
[8] A.J. Pick and D.J. Cole, *Driver steering and muscle activity during a lane-change manoeuvre*, Veh. Syst. Dyn. 45 (2007), pp. 781–805.
[9] A.J. Pick and D.J. Cole, *Dynamic properties of a driver's arms holding a steering wheel*, Proc. Inst. Mech. Eng. D, J. Automob. Eng. 221 (2007), pp. 1475–1486.
[10] A.J. Pick and D.J. Cole, *A mathematical model of driver steering control including neuromuscular dynamics*, Trans. ASME J. Dyn. Syst. Meas. Control 130 (2008), 9pp. 031004.
[11] W. Hoult, *A neuromuscular model for simulating driver steering torque*, PhD thesis, University of Cambridge, 2008.
[12] W. Hoult and D.J. Cole, *A neuromuscular model featuring co-activation for use in driver simulation*, Suppl. Veh. Syst. Dyn. 46 (2008), pp. 175–189.
[13] A.M.C. Odhams, *Identification of driver steering and speed control*, PhD thesis, University of Cambridge, 2006.
[14] A.M.C. Odhams and D.J. Cole, *Identification of a Driver's Preview Steering Control Behaviour Using Data from a Driving Simulator and a Randomly Curved Road Path*, Proceedings of 10th International Symposium on Advanced Vehicle Control AVEC10, Loughborough, UK, 2010.
[15] D.J. Cole, A.J. Pick, and A.M.C. Odhams, *Predictive and linear quadratic methods for potential application to modelling driver steering control*, Veh. Syst. Dyn. 44 (2006), pp. 259–284.
[16] C. Droogendijk, *A new neuromuscular driver model for steering system development,* Master's thesis, Delft University of Technology, 2010.
[17] D. Katzourakis, C. Droogendijk, D. Abbink, R. Happee, and E. Holweg, *Driver Model with Visual and Neuromuscular Feedback for Objective Assessment of Automotive Steering Systems*, Proceedings of 10th International Symposium on Advanced Vehicle Control AVEC10, Loughborough, UK, 2010.
[18] C. Sentouh, P. Chevrel, F. Mars, and F. Claveau, *A Human-Centred Approach of Steering Control Modelling*, Proceedings of 21st IAVSD Symposium on Dynamics of Vehicles on Roads and Tracks, Stockholm, 2009.
[19] D.J. Cole, *Steering feedback: Mathematical simulation of effects on driver and vehicle*, ATZ Autotechnol. 8 (2008), pp. 52–56.
[20] W. Hoult and D.J. Cole, *Steering Feedback: Modelling its Effect on Driver and Vehicle*, Proceedings of Vehicle Dynamics and Control 2009, Cambridge, 2009.
[21] G. Rill, *First order tyre dynamics, in 3rd European Conference on Computational Mechanics Solids, Structures and Coupled Problems in Engineering,* Springer, Lisbon, Portugal, 5th–8th June 2006.
[22] D. Winters, *Biomechanics and Motor Control of Human Movement*, 2nd ed., John Wiley and Sons, Chichester, 1990.
[23] J. Shemmell, M.A. Krutky, and E.J. Perreault, *Stretch sensitive reflexes as an adaptive mechanism for maintaining limb stability*, Clin. Neurophysiol. 121 (2010), pp. 1680–1689.
[24] A.M.C. Odhams and D.J. Cole, *Application of linear preview control to modelling human steering control*, Proc. Inst. Mech. Eng. D, J. Automob. Eng. 223 (2009), pp. 835–853.
[25] R.S. Sharp and V. Valtetsiotis, *Optimal preview car steering control*, Veh. Syst. Dyn. 35 (2001), pp. 101–117.
[26] A.J. Pick, *Neuromuscular dynamics and the vehicle steering task*. PhD thesis, University of Cambridge, 2004.
[27] W. Sardar, *Active vehicle steering and neuromuscular dynamics*. MEng thesis, University of Cambridge, 2009.